Large Eddy Simulation of acoustic pulse propagation and turbulent flow interaction in expansion mufflers

Nishant K. Singh[a], Philip A. Rubini[b*]

[a] *Dept of Mechanical Engineering, Imperial College London, South Kensington, London SW7 2AZ*

[b] *School of Engineering, The University of Hull, Kingston upon Hull, United Kingdom HU6 7RX.*

**Contact authors: n.k.singh@lboro.ac.uk, p.a.rubini@hull.ac.uk.*

Abstract

A novel hybrid pressure-based compressible solver is developed and validated for low Mach number acoustic flow simulation. The solver is applied to the propagation of an acoustic pulse in a simple expansion muffler, a configuration frequently employed in HVAC and automotive exhaust systems. A set of benchmark results for experimental analysis of the simple expansion muffler both with and without flow are obtained to compare attenuation in forced pulsation for various mean-flow velocities. The experimental results are then used for validation of the proposed pressure-based compressible solver. Compressible, Unsteady Reynolds Averaged Navier-Stokes (URANS) simulation of a muffler with a mean through flow is conducted and results are presented to demonstrate inherent limitations associated with this approach. Consequently, a mixed synthetic inflow boundary condition is developed and validated for compressible Large Eddy Simulation (LES) of channel flow. The mixed synthetic boundary is then employed for LES of a simple expansion muffler to analyse the flow-acoustic and acoustic-pulse interactions inside the expansion muffler. The improvement in the prediction of vortex shedding inside the chamber is highlighted in comparison to the URANS method. Further, the effect of forced pulsation on flow-acoustic is observed in regard to the shift in Strouhal number and the energy absorption in the higher modes inside the simple expansion muffler.

Keywords: Low Mach number flow, Noise attenuation, Synthetic turbulence, Compressible Navier-Stokes, URANS, LES.

1. Introduction

Noise continues to be one of the more undesirable by-products from recent advancements in technology. With increasing challenges and complexities in the design process of mechanical devices and stricter environment norms set by governments, the control and reduction of noise has become a greater challenge in recent years. In order to understand the control and attenuation of noise in industry, sound propagation in acoustic devices remains an active research topic. The expansion muffler has been an essential component of the design and development of noise reduction systems for its numerous applications in exhaust silencer and air-conditioning HVAC system and has been extensively studied by many authors, see for example [1,2].

Although there has been significant research activity including both experimental and analytical studies of expansion mufflers, the area of high-fidelity Large Eddy Simulation (LES) or even Direct Numerical Simulation (DNS) of mufflers has been relatively untouched due to the considerable computational requirement and shortcomings in numerical methods. However, as a result of continuing advances in memory and speed of high performance computers, the application of computational simulation to such problems, at least in the form of LES, is becoming viable. An improved understanding of the process will help to explain the interaction of acoustic signals with turbulent flow, the predominant regime for the majority of industrial applications. Despite considerable developments in the field, a number of issues have hindered the growth of computational acoustics based upon the numerical solution of the Navier-Stokes equations. These issues include the disparity in the temporal and spatial scales describing the underlying turbulent flow field and those associated with the propagation of acoustic waves. Incompressible solvers (in comparison to compressible solvers) reduce the computational effort but that saving is achieved at the cost of losing acoustic information from the problem. Such acoustic information is often critical to the problem, especially in understanding the physics of acoustic pulse propagation in various

acoustic devices. For a compressible solver, aero-acoustic noise simulations or turbulent flow simulations require highly resolved spatial and temporal resolution of acoustic phenomena. Furthermore, the governing equations change their mathematical form, the equations for unsteady inviscid compressible flow represent a hyperbolic system with finite wave speed, whereas their incompressible counterpart is hyperbolic-elliptic with infinite propagation rates. This is one reason why many previous time-dependent Computational Acoustic studies have avoided Computational Fluid Dynamics (CFD) methods for simulation of acoustic pulse and instead reduced computational models were applied. However with current advances in parallel computing and CFD techniques, it has become possible to simulate a time dependent computational acoustic problem at low Mach number through the solution of the full compressible Navier-Stokes equations.

It is important to understand the physical interpretation of a low Mach number flow especially with respect to the numerical solution of the Navier-Stokes equations for acoustic problems. In a low Mach number regime, the wave propagation speed is much greater than the mean flow velocity resulting in very rapid propagation of pressure waves. In response to this, rapid pressure equalization takes place which creates a large unsustainable pressure gradient in local flow. This finally results in no change in mean density due to compression and the flow becomes incompressible in the limit, irrespective of the fact that there may still be some large density variations due to non-homogeneous entropy distributions. This necessitates a modified solver algorithm with Mach-uniform accuracy and efficiency, applicable to both compressible and incompressible regimes inside a flow device [3-11].

There have been a number of previous attempts to develop a computational algorithm applicable to both compressible and incompressible flow regimes, see for example [3, 12, 13, 6] and this area of research is not yet closed as further improvements are still possible. An implicitly discretised time dependent non-iterative pressure-based Operator Splitting method, PISO (Pressure-Implicit with Splitting of Operators) was developed by Issa [4]. This method employed the splitting of operators into a series of steps in such a way that the pressure equations are decoupled from the velocity equation at each time step. The fields obtained at each time step are a close approximation of the exact differencing equation with an order of accuracy depending upon the power of number of operator splitting on time-step increment (δt). PISO was also tested for its stability and its applicability to steady and unsteady problems [14-15]. Some semi-implicit methods have previously been implemented for the resolution of acoustic wave in low Mach number flows [16].

Flow attenuation in acoustic devices presents a varied range of mean flow speeds and wave propagation speeds and therefore a unified solver for all flow regions is essential. In the present work, a pressure-based hybrid algorithm, derived from the PISO solver developed by Issa [4] and the low Mach number flow solver developed by Karki [18], is presented and applied to a low Mach aero-acoustic expansion muffler. There has been similar work reported in the recent past to simulate acoustic pulse propagation through expansion chamber using commercial CFD codes [19,20]. However, the solvers employed were found to be computationally stiff and lead to divergence of solutions when a fluctuating random signal was introduced inside the computational domain. Therefore, an attempt is made in the present work to simulate an acoustic pulse in the expansion muffler using a modified, hybrid pressure-based compressible flow solver, instead of the general subsonic flow compressible solver used by typical commercial CFD codes.

Apart from the direct approaches to inspect instantaneous numerical fields, there are other approaches which use statistical or time averaged mean flow quantities of the primary flow

variables. Such averaged (Reynolds Average Navier Stokes) RANS simulations are found to be satisfactory in various applications and reach universal asymptotic behaviour irrespective of initial boundary condition [21]. However the underlying limitations associated with RANS methods, due to averaging of the turbulent scales, accuracy with time advancement and modelling of the full spectrum, presents accurate simulation of acoustic propagation with many inherent difficulties. Unsteady RANS (URANS) on the other hand provides an alternative time advancing solution but still models the full spectrum of turbulent scales in a flow. For these reasons, URANS has limited effectiveness for complex flows where separation and recirculation are present, such as expansion mufflers, cavities and resonators. Direct solution of the Navier-Stokes equations (DNS) could by definition provide accurate results in separating flow cases but would come at a very high computational cost and is not feasible for industrial applications. Large Eddy Simulation (LES), has however been demonstrated to be computationally feasible as a tool to study sound propagation [22-26].

One practical problem for LES simulations is the necessity to represent the structure of the turbulent flow at the inlet to the computational domain. Although an upstream flow condition can ideally provide good inflow data, the computational boundary cannot, however, be extended upstream indefinitely. Although these upstream flow methods, typically employing periodic boundaries or recycling methods are very accurate, they are computationally expensive and are not applicable to most of the flow simulations of practical importance. In the simulation of acoustic propagation in a muffler, for example, lengthy inlet and outlet ducts require considerable computational resource and the recycling of the acoustic information from the downstream to upstream flow is not possible when the objective of the simulation is to evaluate acoustic attenuation. The inlet condition should also be consistent with the turbulence model chosen for simulation. It is therefore preferable to employ a lower order description provided by different related turbulent quantities then to use enormous amount of information to describe turbulence. In some cases, random fluctuations have been superimposed on a uniform inlet velocity to achieve a pseudo-turbulent behaviour at the inlet [27], which helps create something similar to a turbulent flow at the inlet without contaminating the inflow with upstream acoustic information. The generation of random velocity profile for inflow data to match actual turbulent flow field is a difficult and computationally challenging process. In this context, synthetic boundary condition have been found to be a good alternative for generation of inflow condition for LES, for example the spectral method proposed by Davidson and Billson [28] and Davidson et al [29-31].

The objective of the present work is to develop a full compressible Navier-Stokes solution algorithm for acoustic propagation problems. A new hybrid low Mach number pressure based compressible solver is developed to simulate propagation of pulses of random shape, demonstrated by application through a simple expansion muffler. To accurately simulate the interaction of flow-acoustic and flow-turbulence inside the muffler, a mixed spectral method is proposed by extending the spectral method proposed by Davidson and Billson [28] and with a designated temporal correlation, two points spatial correlation and one point cross correlation. The method is applied for LES of simple expansion muffler to avoid any contamination which could have arisen from the upstream recycling methods.

Validation is achieved by comparison with experimental data collected from a dedicated test rig employing extended inlet and outlet sections. As a demonstration of the capability of the solver, the interaction of acoustic pressure waves generated inside an expansion chamber with the turbulent flow is investigated.

2. Computational Method

2.1 URANS and LES Methodology

The instantaneous compressible Navier-Stokes equations may be transformed into either an Unsteady Reynolds Average form (URANS) through application of time averaging or spatially filtered to form a set of equations suitable for Large Eddy Simulation (LES). The resultant equations are summarised below, see [32] for a full description:

URANS Equations:

$$\frac{\partial \bar{\rho}}{\partial t} + \frac{\partial \bar{\rho}\hat{u}_i}{\partial x_i} = 0, \tag{1}$$

$$\frac{\partial \bar{\rho}\hat{u}_i}{\partial t} + \frac{\partial \bar{\rho}\hat{u}_i\hat{u}_j}{\partial x_j} = -\frac{\partial P}{\partial x_j} + \frac{\partial \tau_{ij}}{\partial x_j} + \frac{\partial \bar{\sigma}_{ij}}{\partial x_j}, \tag{2}$$

$$\frac{\partial \bar{\rho}\hat{E}}{\partial t} + \frac{\partial \bar{\rho}\hat{u}_j\hat{h}}{\partial x_j} = \frac{\partial}{\partial x_j}\left(\bar{\sigma}_{ij}\hat{u}_i + \overline{\sigma_{ij}u_i'}\right) - \frac{\partial}{\partial x_j}\left(\bar{q}_j + c_p\overline{\rho u'T'} + \bar{\sigma}_{ij}\hat{u}_i\tau_{ij} + \overline{\rho u'k}\right) \tag{3}$$

$$P = (\gamma - 1)\{\bar{\rho}\hat{E} - \frac{1}{2}\rho(\hat{u}^2 + \hat{v}^2 + \hat{w}^2) - \bar{\rho}k\}$$

Where $\widehat{\ }$ denotes density weighted Favre-averaged variable and $\bar{\ }$ denotes averaged variable. $\bar{\sigma}_{ij}$ is usually modelled by the Boussinesq assumption (provides S_{ij}) and

$$\hat{h} = \hat{E} + \frac{\bar{p}}{\bar{\rho}}$$

$$\bar{q}_j = -\frac{c_p\hat{\mu}}{Pr}\frac{\partial \hat{T}}{\partial x_j}$$

In the Unsteady RANS approach it is assumed that the time averaging process occurs over a period of time sufficiently long to capture the turbulent fluctuations, whilst still short in comparison to large scale temporal changes in the flow field.

LES Equations:

$$\frac{\partial \bar{\rho}}{\partial t} + \frac{\partial \bar{\rho}\hat{u}_i}{\partial x_i} = 0, \tag{4}$$

$$\frac{\partial \bar{\rho}\hat{u}_i}{\partial t} + \frac{\partial \bar{\rho}\hat{u}_i\hat{u}_j}{\partial x_j} = -\frac{\partial \bar{P}}{\partial x_j} + \frac{\partial(\hat{\tau}_{ij} + \tau_{ij,SGS})}{\partial x_j}, \tag{5}$$

$$\frac{\partial \bar{\rho}\hat{E}}{\partial t} + \frac{\partial \bar{\rho}\hat{u}_j\hat{E}}{\partial x_j} = -\frac{\partial \bar{P}\hat{u}_i}{\partial x_j} + \frac{\partial \hat{u}_i}{\partial x_j}(\hat{\tau}_{ij} + \tau_{ij,SGS}) - \frac{\partial}{\partial x_j}\left(\hat{q}_j + q_{j,SGS}\right) \tag{6}$$

where $\widehat{\ }$ denotes density Favre-filtered resolved variable and $\bar{\ }$ denotes filtered variable and

$$\tau_{ij,SGS} = -2\mu_{sgs}S_{ij}$$
$$q_{j,SGS} = -\left(\frac{\mu_t c_p}{Prt}\right)\frac{\partial \hat{T}}{\partial x_j}$$

where μ_t is a sub-grid turbulent viscosity, S_{ij} is the resolved rate of strain, δ_{ij} is the deviatoric constant and Pr_t is turbulent Prandtl number.

Smagorinsky's SGS model is derived from the simplifying assumption that the small scales are in equilibrium and dissipate entirely and instantaneously all the energy received from the resolved scales. (Smagorinsky 1963) Smagorinsky model has the form of:

$$\mu_{SGS} = \rho(C_s\,\Delta)^2\,\left|\overline{S_{IJ}}\right|$$

$$S_{ij} = \frac{1}{2}\left(\frac{\partial u_j}{\partial x_i} + \frac{\partial u_i}{\partial x_j}\right)$$

Where Δ is usually taken as mesh spacing and C_s is the Smagorinsky constant and the value of this parameter has been determined from the isotropic turbulence decay and ranges between 0.18 and 0.23 for such flows.

2.2 Low Mach Number solver

In order to avoid the numerical instability issues associated with simulation of low Mach number compressible flow, a hybrid algorithm (S-K-P) proposed by Singh [32] was implemented in OpenFOAM [33]. The S-K-P algorithm adopts the operator splitting feature of PISO with modified predictor and corrector steps inspired by Karki's [34] derivation of mass-flux at control-volume face and thereby achieving a tighter coupling between predictor and corrector steps. The key feature of the S-K-P algorithm is within the pressure correction step of the PISO algorithm, which for the proposed solver has the form,

$$\Delta_i\left\{\left(\frac{1}{\delta t} - \frac{A_0}{\rho^n}\right)^{-1}\Delta_i - \frac{\varphi(p,T)}{\delta t}\right\}(p^* - p^n) = \Delta(\rho^n u_i^*) + K\,\Delta_i(p^* - p^n)u_i^* \qquad \ldots (7)$$

The correction step is different from the typical PISO solver in terms of an additional pressure gradient term and works both as relaxation factor as well as Mach number correction factor (See [32] for full derivation).

2.3 Verification

The propagation of an acoustic pulse through a simple expansion muffler is applied to demonstrate the effectiveness of the proposed S-K-P algorithm in a compressible flow solver.

The working fluid was defined to be air, at atmospheric temperature and pressure, modelled as an ideal gas. A pure single period sinusoid, with a time period of 0.3125µs, equivalent to a 3200 Hz frequency and amplitude of 0.05 m/s was superimposed upon a zero mean velocity at the inlet of the expansion muffler. The computational domain was defined to include an extended inlet and outlet, fourteen times the length of the expansion section, as recommended by [19]. This was adopted to ensure an appropriate wave propagation time would be possible, such that a sufficient amount of data to obtain reasonable results could be obtained (see Figure 1). The outlet was defined as non-reflective in order to avoid spurious reflections from

the boundary. The outlet pressure was defined as a constant total atmospheric pressure (Dirichlet boundary condition for velocity). The wall shear stresses due to viscous forces were included in the compressible solver calculations and heat transfer at the walls of the domain was neglected. Second order Gauss linear was employed for spatial discretization of the diffusion and convection terms and second order Crank Nicolson temporal discretization was employed throughout the simulations.

A mesh spacing of 4 mm or smaller was adopted for the majority of the simulations in order to provide sufficient spatial resolution of the pressure waves at the wavelengths of interest. As a consequence, a time step of not greater than 5μs was required to maintain a maximum Courant number of unity. This equates to a maximum sampling frequency of 200 kHz and Nyquist frequency of 100 kHz. The corresponding wavelength at this Nyquist frequency is 3.4 mm, which is less than than the mesh spacing of 4 mm, therefore the solver will be unable to resolve frequencies above the Nyquist frequency and aliasing should not be an issue.

In this study, transmission loss was adopted as the quantitative parameter to assess acoustic attenuation. Transmission loss is defined as the difference between the sound power incident at the entry of the filter (or muffler) and the sound power transmitted after the muffler and is defined as follows,

$$TL = 10\log\left(\frac{W_{inc}}{W_{tra}}\right) = 20\log\left(\frac{P_{inc}}{P_{tra}}\right) \quad \text{... (8)}$$

Where p_{inc} and p_{tra} are the amplitudes of incident and transmitted waves in the muffler, see Figure 1, and the square of these amplitudes are proportional to the sound intensities, W_{inc} and W_{tra}. The inlet and outlet sections were extended to fourteen times the length of expansion section; this allowed data to be collected over a sufficient time period in the absence of any unwanted reflections. Within this time period the above definition of Transmission Loss is equivalent to that in the presence of anechoic terminations. The mesh for the expansion muffler is shown in Figure 2.

The mesh dependence of the simulation was confirmed by comparison of results over a range of mesh sizes from 4 mm to 1 mm. Fast-Fourier (FFT) analysis of the time series acoustic pressure was performed. Figure 3(a) presents a comparison of transmission loss for the different mesh sizes. The results for each successively refined mesh display comparable agreement with no significant discrepancies. However, although a good agreement can be seen up to a frequency of 2500Hz, finite volume acoustic simulations are vulnerable to spatial and temporal discretization error at higher frequencies, as illustrated in Figure 3(b). Figure clearly demonstrates significant grid dependency as the frequency increases. This is due to the inability to resolved higher frequencies on coarse meshes. The propagation of sinusoidal propagation through expansion chamber is shown as velocity contours in Figure 4.

3. Validation Experiment

3.1 Experiment configuration

A series of experiments were undertaken to provide quantitative data for validation of the computational simulations. Figure 5 illustrates the experimental configuration with all the listed equipment, devices and software used in this experimental investigation. A 22kW ACI Centrifugal Fan was employed to drive the flow duct. A signal generator (Thandar TG503, 5MHz pulse generator) was employed for signal generation, after amplification the signal was propagated through the duct via a Fane Crescendo mid-bass loudspeaker driver designed

to exhibit smooth frequency responses. The signal interacts with the expansion section of the muffler and changes in impedance were recorded. The incident and transmitted signal before and after the expansion was recorded using Brűel & Kjær Type 4134 microphones, as shown in Figure 5. The resultant signals were then passed through Brűel & Kjær Type 2609 microphone amplifiers passed on to the Signal analyser. The signal analyser was connected with the digital computer with LabVIEW software interface to save the recorded signal in a data file. Signal analysis was performed with Matlab software using Fourier transform to represent the time series signal in a frequency domain.

3.2 Comparison of Experiment and simulation – zero mean flow

A baseline configuration was obtained by recording the acoustic response from a configuration with an inlet pipe and no expansion, essentially a straight through flow duct. The resultant pressure response is illustrated in Figure 6, this was then employed as the inlet boundary condition for the computational solver in the presence of the simple expansion muffler geometry. Pressure response data was recorded at the two microphone locations close to the inlet and downstream from the expansion chamber. The pressure data was then Fourier transformed to obtain a transmission loss spectrum and comparisons were then made with the experimental results to analyse the attenuation due to the presence of the simple expansion muffler.

A comparison of the transmission loss spectrum and transmitted pressure pulse for a generator frequency of 500 Hz is shown in Figure 7. The transmission loss spectrum predicted by the S-K-P compressible solver clearly captures all of the attenuation peaks in the frequency domain. The prediction of the propagation of the pressure pulse also agrees well with the experimental pulse, though some effects of a numerically induced phase error are apparent. As a transient finite volume compressible flow solver, the prediction capability of the solver for a random mix of frequencies as input was deemed encouraging. The stability of the solver was found to be very good throughout the pulse propagation and all the high frequency pressure pulses were captured by the solver. The prediction demonstrates the ability of the S-K-P solver to represent the low Mach number acoustic flow simulation and capture all the available high frequency components in the solution.

Comparison between experiment and simulation provides a useful observation regarding the capability of this low Mach number flow solver. Defining “Effective Transmission Loss” as the normalised difference between the transmission loss for experiment and simulation, representing the discrepancy between simulation and experiment. Figure 8, provides the Effective transmission loss for a 500Hz signal frequency which demonstrates good agreement at lower frequencies although slightly higher discrepancies at higher frequencies. For lower frequency range the discrepancy varies to about 5-7%, whereas for higher frequency ranges it goes as high as 25%.

3.3 Effect of mean flow

A set of experiments were conducted for a simple expansion muffler with a mean through flow velocity of 10 m/s inside the chamber. The same random mix of pressure pulses (as in section 3.2) was imposed over the mean flow at the inlet of the simple expansion muffler. The acoustic data was collected after the expansion chamber of the simple expansion muffler and also separately for a simple pipe without expansion in the presence of imposed mean flow. The recorded data was calibrated and Fourier transformed to obtain transmission loss spectrum. Figure 9 shows the comparison of transmission loss spectrum for imposed pulse at 500 Hz generator frequency with 10 m/s flow velocity and without any flow. The comparison

shows a consistent level of attenuation throughout the frequency range. However it is important to note that the attenuation at very lower range of spectrum is more pronounced than the higher range of spectrum. In other words, the attenuation in the lower frequency ranges for the no-flow condition is less pronounced and rather a higher attenuation in that range is observed due to the consistent attenuation throughout the spectrum after the introduction of mean flow. A similar observation for the same range of acoustic frequencies was observed by Rupp et al [35] in their investigation of flow through an orifice.

4. Acoustic Simulation of Muffler with mean flow

4.1 RANS simulation

A simple expansion muffler was studied in the previous section in the absence of mean flow. In this section results from a mean flow URANS simulation are presented using a standard k-ε turbulence model [36], to capture length scales of flow and acoustics. A three-dimensional simulation was conducted for a 10 m/s mean flow using the S-K-P compressible solver with 4 mm mesh spacing. As illustration, the predicted RANS mean axial velocity contour is shown in Figure 10.

The transmitted pressure waves from the expansion chamber were recorded at a location close to the inlet and a location immediately downstream from the expansion, as shown in Figure 5 (marked '*a*' and '*b*'). The recorded pressure data was Fourier transformed to obtain transmission pressure pulse and transmission loss spectrum as shown in Figure 11(a) and 11(b). The transmission loss spectrum shows reasonable attenuation at the lower frequency range in comparison to other high fidelity methods (See Figure 15 and 16). The transmission pressure plot also captures the large peaks in the spectrum which corresponds to the lower frequency signals. If a comparison of transmission pressure pulse is made with the zero mean flow case in Figure 3, it is evident that the high frequency component of the pulse is either lost with the mean flow interactions or gets averaged by the numerical method. So, although the numerical method captures all the attenuation peaks in the simulation, there seems to be a trend of increasing attenuation for higher frequency range, which could be either due to discretization error in the numerical method or the dissipation and turbulence modelling error. Despite these discrepancies due to numerical averaging in URANS methods, the method provides reasonable agreement in the lower frequency range and also predicts the attenuation frequency at correct level. The averaging in URANS methods further restrict the scope of the work and was found to be limited to lower frequency analysis.

4.2 Large Eddy Simulation

A three-dimensional Large Eddy Simulation was carried out on the same muffler geometry to ensure good agreement for detailed analysis of the muffler. A mean flow of 10 m/s (Mach number of 0.03) was considered throughout the simulations and once a stationary steady flow had been achieved, a sinusoidal pulse was imposed upon the inlet. In this simulation, acoustic pressure was defined as the spatially varying difference of total pressure and mean pressure inside the chamber. Such a definition of acoustic pressure provides a valuable tool for visualisation of pressure pulse propagation inside the simple expansion muffler. In general, the semi-empirical formula of Rossiter [37] for calculation of Strouhal number St is obtained as,

$$St = \frac{fL}{U} = \frac{n - \varsigma}{M + {}^{1}/_{k}}$$

The Strouhal number calculation for acoustically excited resonance in muffler has been obtained from Desantes et al [38] in present calculations as,

$$St = \frac{fL}{U} = \frac{nH(1 - M^2)}{2ML_c}$$

where f is the vortex-shedding frequency, L_c is characteristic acoustic length, U is flow velocity, M is flow Mach Number, H is height of expansion, k is the ratio of convection velocity of the vortices to the free stream velocity, ς is a factor to account for the time lag between of a vortex and the emission of a sound pulse at the trailing edge of cavity and n is mode number.

4.2.1 Numerical schemes: A second order accurate, limited, linear blended differencing scheme, see Singh [32], was employed for spatial discretization. A Crank-Nicholson second order temporal discretization was employed for all simulations. The blended spatial differencing and mixed Crank-Nicholson scheme helps in stabilising the stiffness present when solving the compressible Navier-Stokes. The S-K-P algorithm proposed by Singh [32] further enhances the robustness of the solver and extends the temporal discretization to operate at fully-implicit time marching scheme. This is particularly helpful in reducing temporal discretization errors introduced during simulation of forced pulse propagation in muffler.

4.2.2 Mesh refinement: Numerical error is a function of mesh size, hence the mesh size for the computational domain should be kept at the minimum possible to reduce numerical error. A 4 mm mesh was again adopted due to acoustic and LES simulation requirements for appropriate resolution of the flow and acoustic length scales (See Figure 2). With the S-K-P algorithm, it was found that the 4 mm mesh along with synthetic boundary condition for LES model provided accurate results for acoustic propagation in the simple expansion muffler. Wall grading was employed near the pipe wall and a no-slip condition was employed instead of wall functions or similar techniques [39]. The no-slip condition was employed to avoid error introduced into the solution domain due to wall-function modelling. The resultant computational mesh corresponded to approximately 2.5 million mesh points for the 3D simulations.

4.2.3 Boundary condition: The boundary conditions were defined as previously described for the URANS simulation, except for the representation of the inlet velocity boundary condition which was defined as a combination of a time varying sinusoidal pulse, a mixed form of synthetic turbulence and a synthetic pulsating boundary. This mixed form of inlet boundary was formulated, whilst retaining the initial boundary requirements for LES simulations in a developing flow. The synthesised turbulent fluctuations, see Singh [32], are given by,

$$v'_i(x)^m = \boldsymbol{a}\, v'_i(x)^{m-1} + \boldsymbol{b}\, \widetilde{v'}_i(x)^m \qquad \ldots (9)$$

The above turbulent fluctuation along with a forced acoustic pulse is superimposed on the mean flow. The forced pulse was defined by,

$$u_f = A\,sin(2\pi ft) \quad \ldots (10)$$

The final time varying velocity inlet boundary was defined by considering the turbulent intensity for the pulsating sinusoidal and imposed on mean flow as follows,

$$U = U_0 + u_f + (1 + \xi)v'_i \quad \ldots (11)$$

Where U_0 is the mean-flow velocity and ξ is the turbulent intensity. The amplitude of the forced pulsation, A, was defined as 0.5 m/s. A non-reflective boundary condition was adopted at the outlet, equivalent to a perfect anechoic termination

4.2.4 Acoustic Simulation: The simulation of a forced pulse with zero mean flow was described earlier. A simple expansion muffler was also simulated with mean flow using URANS to obtain spectral analysis of attenuation in muffler. However, it was found that URANS usually tends to dissipate high frequency information in the computational domain, leading to disparity and discrepancies in the predicted attenuation for higher frequency ranges. In these simulations a 3000Hz sinusoidal pulse was imposed at the inlet of muffler for the purpose of a Large Eddy Simulation of the acoustic propagation.

A similar flow acoustic analysis was undertaken in the domain of the computation by selecting four probes at defined locations (see Figure 1) in the muffler. The first probe (No. 3) was located near the inlet of the expansion wall inside chamber at 7.6m downstream, the second probe (No. 4) was located at the centre of the middle of the expansion, the third probe (No. 2) was located at the far end of the chamber at 8m downstream and the fourth probe (No. 1) was located in the tailpipe of the muffler at 8.2 m downstream from the inlet. The instantaneous pressure, density and velocity data were recorded throughout the period of pulse propagation at each four probe locations, near the front wall of expansion, near the rear wall of the muffler, in the middle of the muffler and in the tailpipe immediately after expansion. The pressure response spectrum $\left(\frac{p^2}{\rho U^2}\right)$ for stationary steady flow for probe No. 1 and 2 are shown in Figure 13. The pressure response spectrum for probes 3 and 4 are found to be very similar to probes 2 and 1, with an exception that the probe 4 has a slight shift in response peak for Strouhal number. Some degree of distinction in the location of peaks can be explained with the dependence of the analytical formulation on local flow Mach number, which considerably fluctuates inside the expansion chamber. It can also be noted in this context that the Mach number of 0.03 at inlet decelerates inside the expansion chamber to a lower than 0.03 average Mach number and therefore analytical formula do not predict the exact location of Strouhal number. Some interesting changes are observed at the far end of the expansion chamber where the flow impinges upon the wall and enters the contracted pipe.

The pressure response spectrum for the probe No. 2 near the far end of the expansion, Figure 14, shows the interference of chamber resonance (calculated using Desantes formulation) and forced pulsation that is introduced later on. The pressure response spectrum for probe No. 2 at the far end of the expansion in Figure 14 shows the presence of higher modes, occurring primarily at Strouhal number of 0.4. These higher modes of chamber resonance are mostly due to change in impedance inside the chamber and also the frequent reflections that may energise the higher modes of the chamber. These mechanism of interaction of the chamber resonance and forced pulsation involves the vortex near the rear wall of chamber that sheds or interacts with the incoming forced pulse and their subsequent reflections. The velocity contour in Figure 12 and Figure 14 clearly indicates the formation of vortex rolls very close to the rear wall of muffler after the pulse crosses the expansion inside the muffler. A

comparison between the velocity contour before pulsation (Figure 13) and velocity contour after pulsation (Figure 14) also supports the formation of vortex at the corner of rear wall.

Pressure response spectrum for probe No. 1 is illustrates a number of phenomena. In addition to the vortices that roll up from the front end of the chamber, there are additional vortices that are generated at the far end (probe 1 and 2) of the expansion where flow enters the contraction and generates vortices, as shown in the velocity contours in Figure 12, 13 and 14. Further inspection of the isosurface plots shown in Figure 12 also highlights the presence of high velocity, closely spaced isosurfaces near the rear wall and contraction pipe junction of the expansion chamber. The pressure spectrum for probe 1 also has an interesting trend with Strouhal number in Figure 14. The amplitude of the pressure response is decreasing for higher modes which are different from the trend shown by the probe 2 where pressure response remains same for all higher modes. Rupp et al [39] argued in his investigation of flow through an orifice that the vortices generated at the entrance of the orifice absorb acoustic energy as kinetic energy of vortex's velocity field and help attenuate noise. The decreasing trend in pressure response spectrum shown in Figure 14 supports the argument of Rupp et al. It is interesting to add in the current argument that the vortices generated from the roll up have far lesser impact on attenuation then the vortices generated at the orifice entrance.

Figure 15 compares the transmission loss spectrum for URANS and LES simulation in the expansion muffler at a forced inlet frequency of 3000 Hz. The large discrepancy at higher frequency range between the URANS and LES simulations can be readily seen, where the URANS approach is unable to resolve higher frequency components due to excessive dissipation and the effect of the underlying time averaging in the URANS simulation. This is also evident when comparing Figure 16 and Figure 11(a).

To better understand the acoustic response of a simple expansion muffler for a range of frequencies, a detailed acoustic response analysis was performed. The mean flow profile of a simple expansion muffler was forced with a range of frequencies, and the acoustic response was recorded to obtain the transmission loss spectrum and transmission pulse plot in the tailpipe. Figure 17 illustrates the transmission loss spectrum and transmission pulse plot for imposed acoustic signals ranging from 500 Hz to 2000 Hz. As is evident from Figure 17 (a), the attenuation inside the simple expansion muffler for pure sinusoidal sound propagation has higher attenuation at their natural sinusoidal frequency than at other frequencies. Figure 17 (b) shows the comparison of the transmitted pressure signals after the expansion. This is consistent with the experimental trend observed in Figure 9. This phenomenon cannot be accurately captured either by Simulations conducted with zero mean flow case or by the URANS compressible solver simulations where the model of turbulence and numerical method itself had some limitations. The better capturing of various acoustic scales and acoustic attenuation in the present work is due to the fact that the current LES simulation of sound propagation in muffler captures turbulence scales and flow separation effects more accurately than the previous simulations done in section 2.

5. Conclusion

A novel hybrid pressure-based compressible solver has been developed for low Mach number acoustic flow simulation. The solver has been applied to the propagation of an acoustic pulse in a simple expansion muffler, a configuration frequently employed in HVAC and automotive exhaust systems. The hybrid low Mach number pressure based compressible solver was validated against a set of experimental data for propagation of an acoustic pulse

through a simple expansion muffler, designed to minimise upstream and downstream reflections. Comparison between experiment and simulation has been shown to be very satisfying.

The simulation of a simple expansion muffler using both a compressible solver with zero mean flow and a URANS turbulent compressible solver with considerable mean flow, provided encouraging results for pulse propagation. The simulations captured the attenuation peaks in the transmission spectrum accurately with acceptable shift in frequency values for lower ranges of frequencies. However, for URANS simulation of an expansion muffler, the limited ability to resolve high frequencies within the computational domain was demonstrated and the limitation of URANS in the application of acoustic simulations of pulse propagation was observed.

The lack of resolution of high frequencies within the computational domain could be attributed to the averaging nature of the URANS method and excessive underlying dissipation from the RANS turbulence model. LES simulation of an expansion muffler using a mixed synthetic boundary condition for the inflow alleviated this issue and successfully captured the high frequency waves inside the computational domain.

Analysis of flow acoustics inside the muffler indicated that the chamber resonance occurred at a Strouhal number of 1.1, for a Mach number of 0.03. Forced pulsations of various frequencies were imposed at the inlet of the simple expansion muffler for the LES simulation and it was found that the interaction of vortices with the acoustic waves impacts the attenuation of the higher modes of the acoustic waves. The effect of orifice vortices was found to be more pronounced on higher modes of oscillations in comparison to the roll up vortices.

Additionally, the experimental analysis of a muffler for various mean flow velocities provides a set of benchmark results which show higher attenuation in transmission loss for considerable mean flow in the muffler. This higher attenuation is proposed to be due to the interaction of turbulence with mean flow acoustic wave propagation. The analysis also provided a comparison for muffler attenuation for various generator pulses with a mean flow. It was found that the trend in the attenuation inside the simple expansion muffler for LES of forced pure sinusoidal sound propagation had higher attenuation at their natural sinusoidal frequency itself than at other frequencies. The attenuation was primarily due to the absorption by the vortex inside the chamber and the vortices generated at the far end of the contraction entrance to pipe. Some of the simulations were also supported and consolidated with experiments.

Acknowledgement

The University of Hull is acknowledged for the support in making this research possible through a research studentship award.

References

[1] D. Suwandi, J.M. Middelberg, K.P. Byrne, N.J. Kessissoglou, Predicting the Acoustic performance of mufflers using Transmission Line theory, Proc. Acoust 2005, 9-11 November 2005; 181-187.

[2] M.L. Munjal, Plane wave analysis of side inlet/outlet chamber mufflers with mean flow. Appl Acoust 1997; 52(2):165-175.

[3] F.H. Harlow, A.A. Amsden, Numerical calculation of almost incompressible flow, J Comp Phys. 1968; 3: 80-93.

[4] R.I. Issa, Solution of the implicitly discretised fluid flow equations by Operator-splitting, J Comp Phys. 1985; 62: 40-65.

[5] E. Turkel, Preconditioned methods for solving the incompressible and low speed compressible equations, J Comp Phys. 1987; 72(2):277-298.

[6] C.L. Merkle, Y. Choi, Computation of low-speed compressible flows with time-marching procedures. Int J Num Meth Eng. 1988; **25**:293-311.

[7] H. Nessyahu, E. Tadmor, Non-oscillatory central differencing for hyperbolic conservation laws, J Comp Phys 1990; 87(2):408-463.

[8] O.C. Zienkiewicz, R. Codina, A general algorithm for compressible and incompressible flow- Part I. the split, characteristic-based Scheme, Int J Num Meth Fluids. 1995; 20: 869-885.

[9] A. Kurganov, E. Tadmor, New high-resolution central schemes for nonlinear conservation laws and convection-diffusion equations, J Comp Phys. 2000; 160: 241-282.

[10] M.F. Webster, I.J. Keshtiban, F. Belblidia, Computation of weakly-compressible highly-viscous liquid flows, Engg Computations 2004;1(7):777-804.

[11] V. Moureau, C. Berat, H. Pitsch, An efficient semi-implicit compressible solver for large-eddy simulations. J Comp Phys. 2007; 226(2) 1256-1270.

[12] F.H. Harlow, A.A. Amsden, A numerical fluid dynamics calculation method for all flow speeds, J Comp Phys. 1971;8:197-213.

[13] A.J. Chorin, A numerical method for solving incompressible viscous flow problems. J Comp Phys. 1967; 2:12-26.

[14] R.I. Issa, A.D. Gosman, A.P. Watkin, The computation of compressible and incompressible recirculating flows by a non-iterative implicit scheme, J Comp Phys. 1986; 62:66-82.

[15] R.I. Issa, B. A-Befrui, K.R. Beshay, A.D. Gosman, Solution of the implicitly discretised reacting flow equations by operator-splitting, J Comp Phys 1991;93: 388-410.

[16] C. Wall, C.D. Pierce, P. Moin, A Semi-implicit Method for Resolution of Acoustic Waves in Low Mach Number Flows, J Comp Phys. 2002;181:545-563.

[17] D.M. Hawken, H.R.T-Jahromi, P. Townsend, M.F. Webster, A Taylor-Galerkin-based algorithm for viscous incompressible flow, Int J Num Meth Fluids 1990;10:327-351.

[18] K.C. Karki, S.V. Patankar, Pressure based calculation procedure for viscous flows at all speeds in arbitarary configurations. AIAA 1989;**27**:1167-1174.

[19] J.M. Middelberg, T.J. Barber, S.S. Leong, K.P. Byrne, E. Leonardi, Computational Fluid Dynamics analysis of the acoustic performance of various simple expansion chamber mufflers, Proc. Acoustics 2004, 3-5 November 123-128.

[20] J. DeSpirito, M.S. Binseel, Modeling of acoustic pressure waves in Level-dependent Earplugs. ARL report 2008; ARL-TR-4607.

[21] W.K. George, L. Davidson, Role of Initial Conditions in Establishing Asymptotic Flow Behavior, AIAA 2004;42(3):438-446.

[22] P. Comte, M. Haberkorn, G. Bouchet, V. Pagneux, Y. Auregan, Large-Eddy Simulation of acoustic propagation in a turbulent channel flow, in: E. Lamballais, R. Friedrich, B. J. Geurts, O. Métais, Direct and Large-Eddy Simulation VI. Springer Sc., Netherlands, 2006; 521-528.

[23] G. Rubio, W. D. Roeck, W. Desmet, M. Baelmans, Large Eddy Simulation for computation of Aeroacoustic sources in 2D-Expansion chambers, in: E. Lamballais, R. Friedrich, B. J. Geurts, O. Métais, Direct and Large-Eddy Simulation VI. Springer Sc., Netherlands, 2006; 555-564.

[24] A. Roux, L.Y.M. Gicquel, Y. Sommerer, T.J. Poinsot, Large eddy simulation of mean and oscillating flow in a side-dump ramjet combustor. Comb. Flame 2008; 152: 154-176.

[25] F. Mendonca, A. Read, S. Caro, K. Debatin, B. Caruelle, Aeroacoustic simulation of double diaphragm orifices in an aircraft climate control system, AIAA Aeroacos. Conf. 23-25 May 2005.

[26] A. Roux, G. Lartigue, T.J. Poinsot, U. Meier, C. Berat, Studies of mean and unsteady flow in a swirled combustor using experiments, acoustic analysis, and large eddy simulations. Comb. Flame 2005;141:40-54.

[27] M.M. Rai, P. Moin, Direct numerical simulation of transition and turbulence in a spatially evolving boundary layer. Journal of Computational Physics 1993;109: 169-192.

[28] L. Davidson, M. Billson, Hybrid LES/RANS using synthesized turbulence for forcing at the interface. Int J Heat Fluid Flow 2006;**27**(6) :1028-1042.

[29] L. Davidson, Hybrid LES-RANS: Inlet boundary conditions for flows including recirculation. Int S Turb Shear flow Phen, Munich 2007; 689-694.

[30] L. Davidson, Using isotropic synthetic fluctuations as inlet boundary conditions for unsteady simulations. Adv Appl Fluid Mech, 2007;109:1-35.

[31] L. Davidson, S. Dahlstrom, Hybrid LES-RANS: An approach to make LES applicable at high Reynolds number. Intl. J. Comp. Fluid Dyn, 2007; 19: 415-427.

[32] N.K. Singh, Large Eddy Simulation of Acoustic Propagation in Turbulent Flow through Ducts and Mufflers. PhD thesis, U Hull, 2012.

[33] OpenFOAM, OpenFOAM-The Open Source CFD Toolbox: Users Guide, Programmers Guide, 2007.

[34] K.C. Karki, A calculation procedure for viscous flows at all speeds in complex geometries, PhD Thesis, U Minnesota, 1986.

[35] J Rupp, J Carrotte, A Spencer, Interaction between the acoustic pressure fluctuations and the unsteady flow field through circular holes. J Eng Gas Turbines Power 2010; 132(6): 061501-1–1-9.

[36] WP Jones, B E Launder, The prediction of laminarization with a two-equation model of turbulence. Intl J. Heat M Trans, 1972; 15(2):301-314.

[37] JE Rossiter, Wind tunnel experiments on the flow over rectangular cavities at subsonic and transonic speeds, Aeronautical Research Council Reports and Memoranda 01/1964; No. 3438.

[38] JM Desantes, AJ Torregrosa, A Broatch, Experiments on Flow Noise Generation in Simple Exhaust Geometries. Acta Acustica united with Acustica, 2001; 87(1), pp. 46-55.

[39] JW Deardorff, A numerical study of three-dimensional turbulent channel flow at large Reynolds number. J Fluid Mech, 1970; 41(2):453-480.

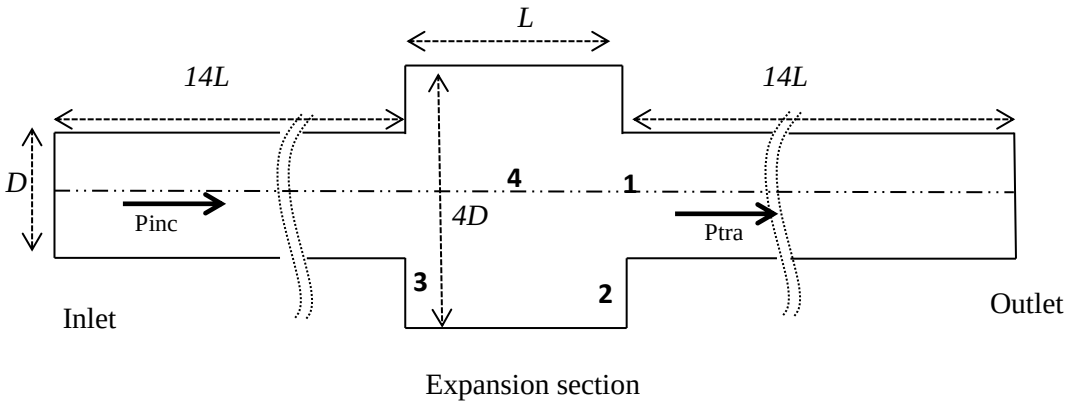

Figure 1: *Geometry of Simple Expansion Muffler (of length L)*

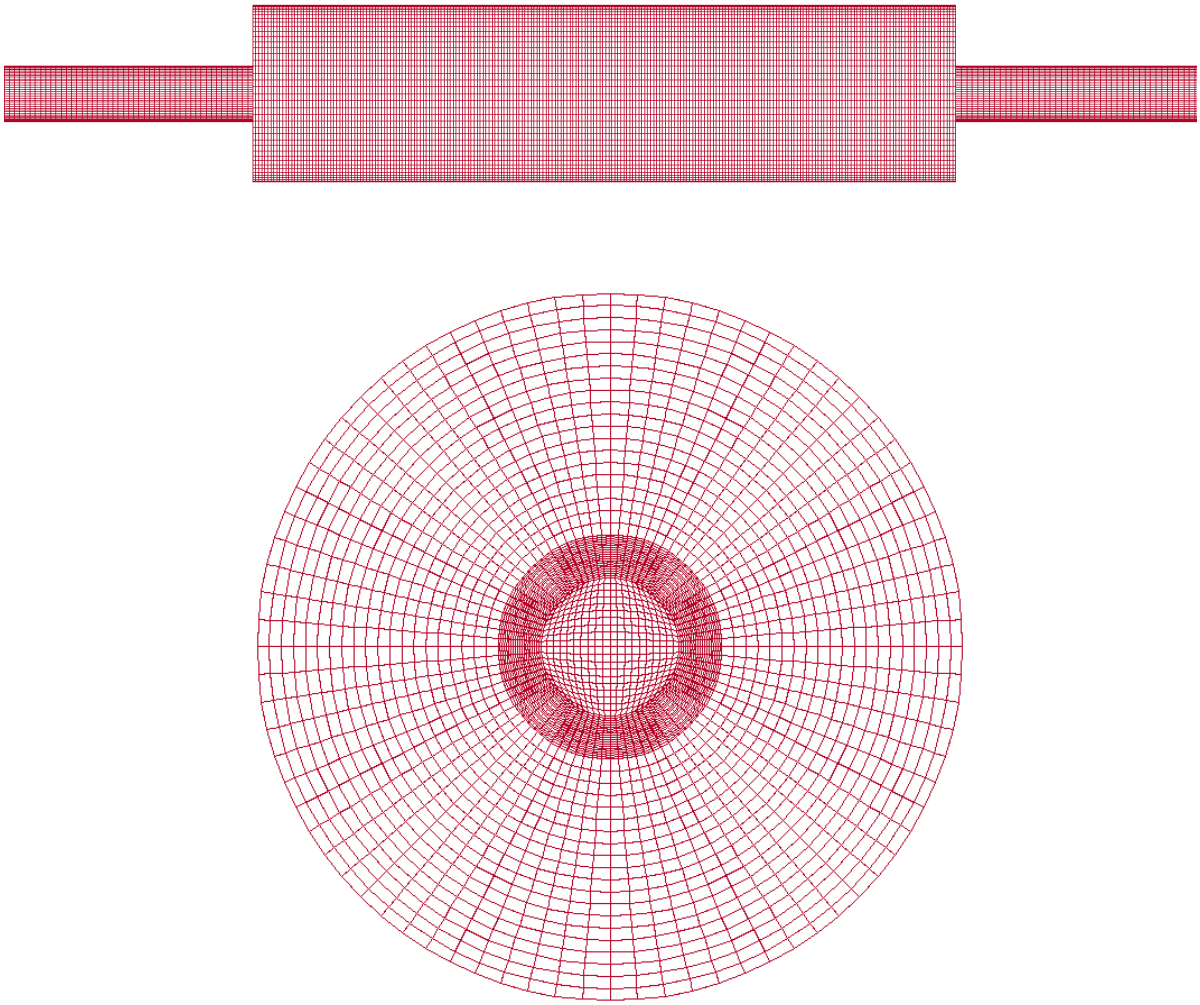

Figure 2: *Simple Expansion Muffler 3D Mesh: Front View (top) and Side View (bottom)*

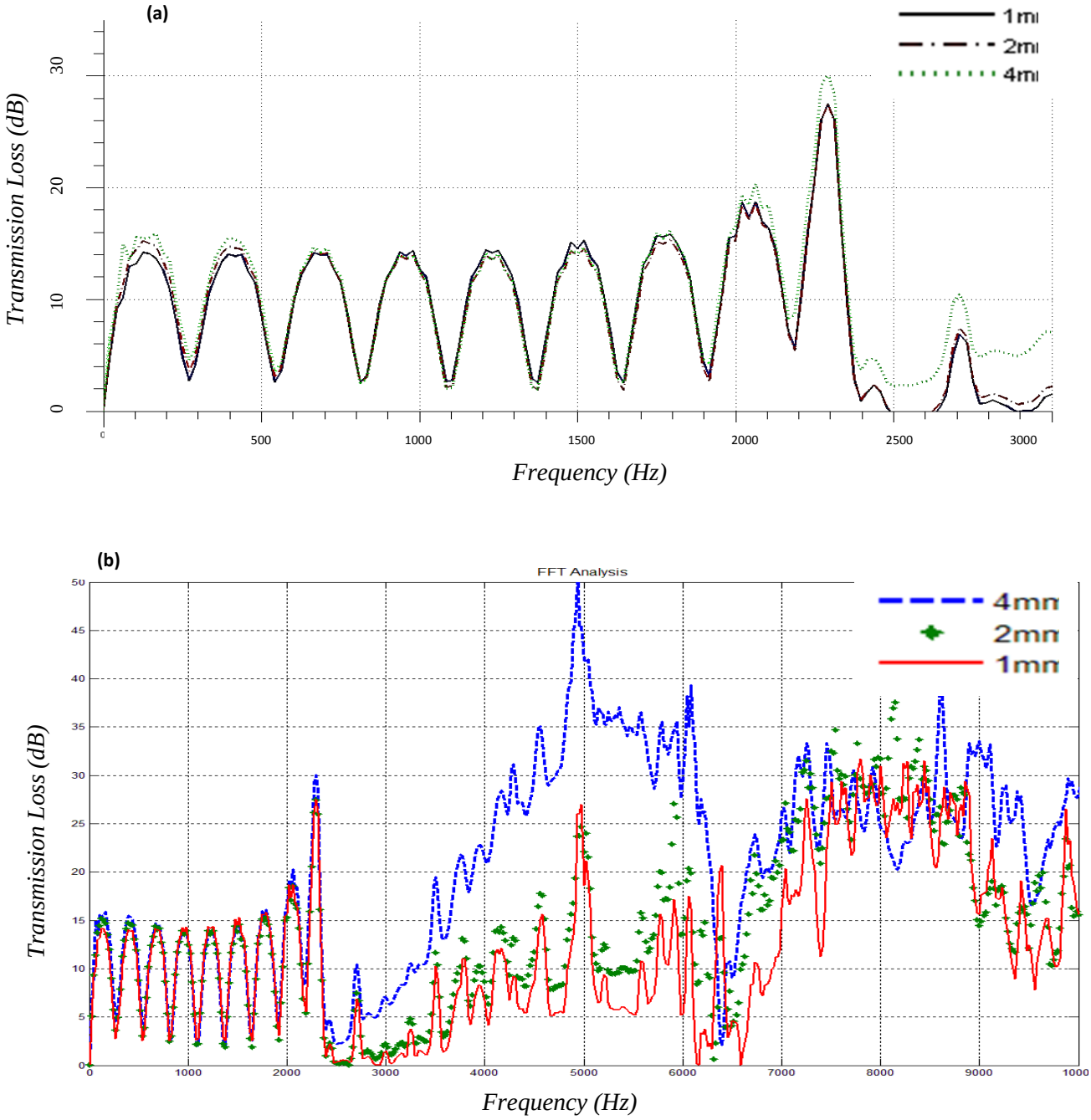

Figure 3*: *(a) *Predicted transmission loss and effect of mesh resolution.* ***(b)*** *Extended spectrum of (a) in higher frequency range.*

(a)

(b)

(c)

(d)

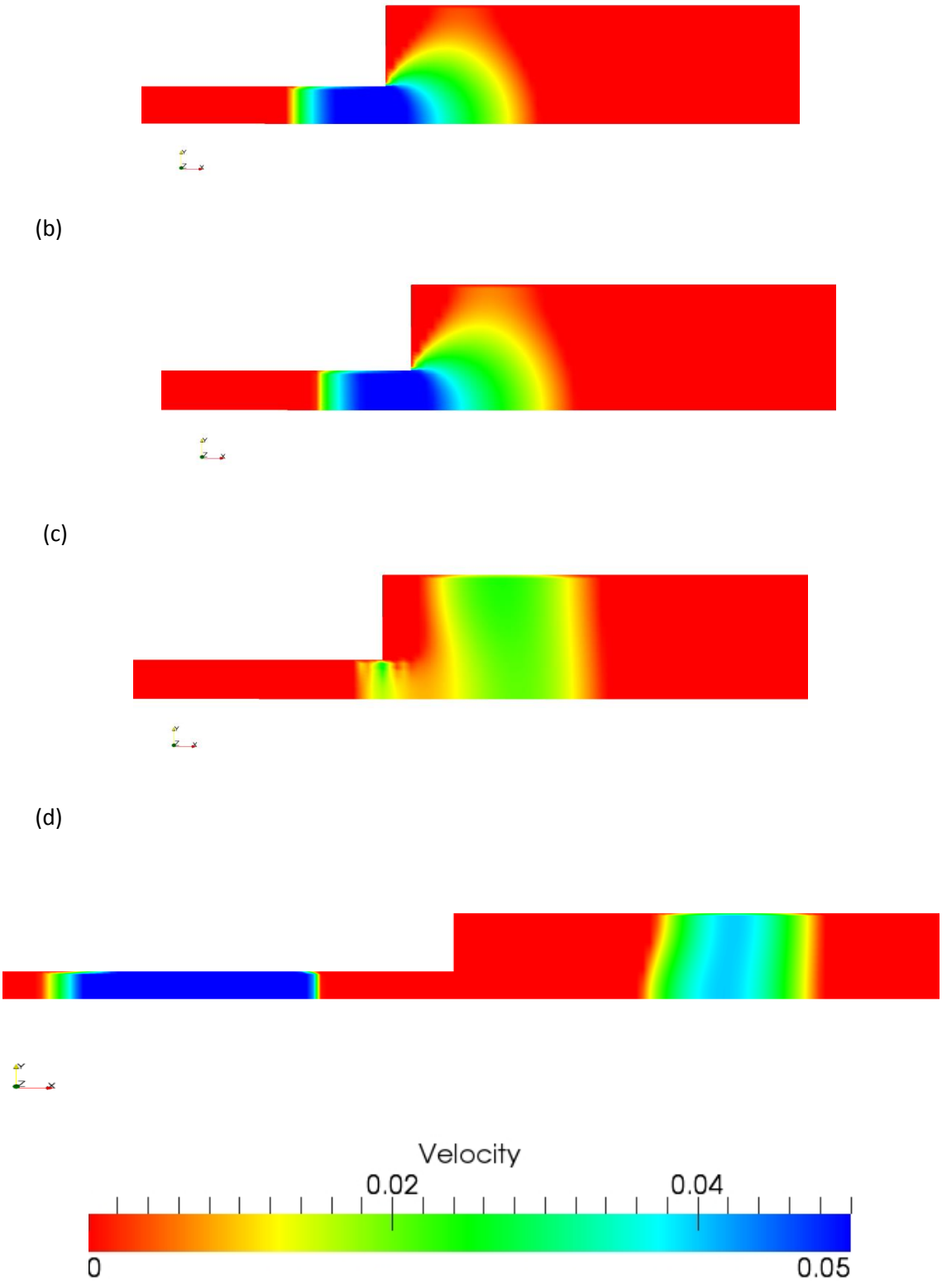

Figure 4: *Axial Velocity (m/s) contours at start of expansion: (a), (b) Sinusoidal pulse reaches at entrance of expansion chamber, (c), (d) Reflection and propagation of pulse from the expansion section.*

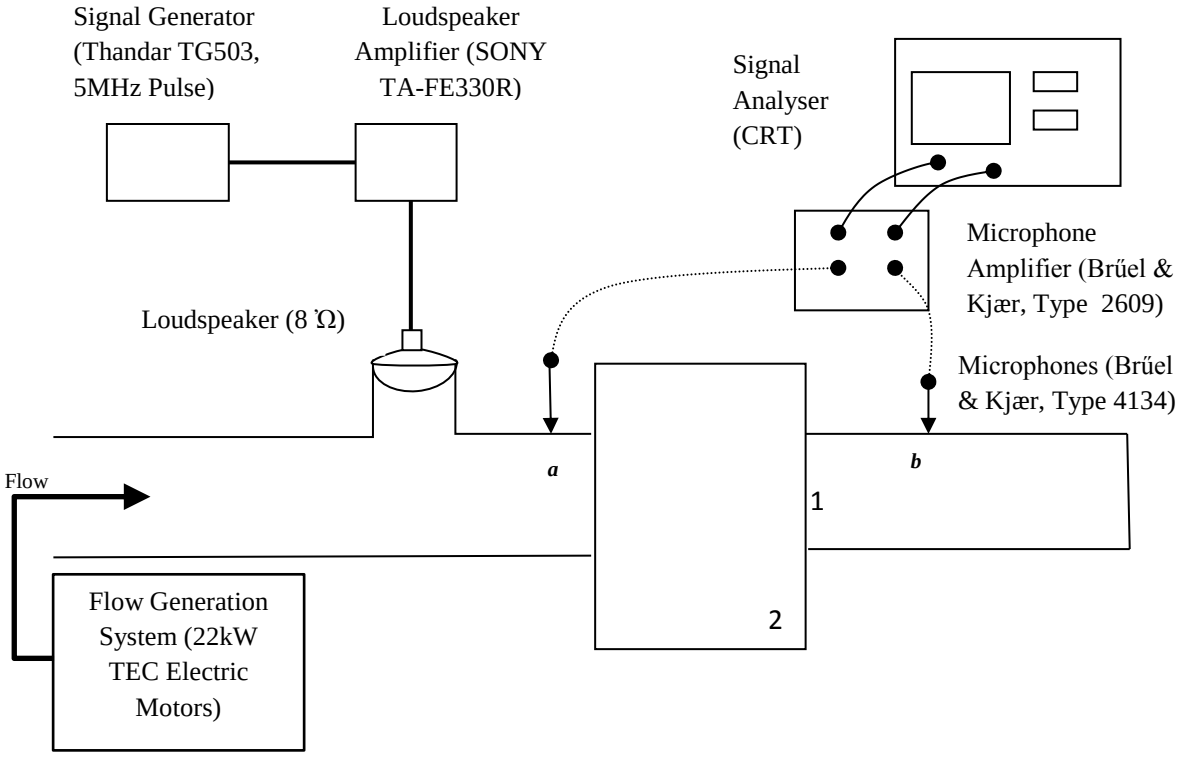

Figure 5: *Schematic diagram of experimental facility*

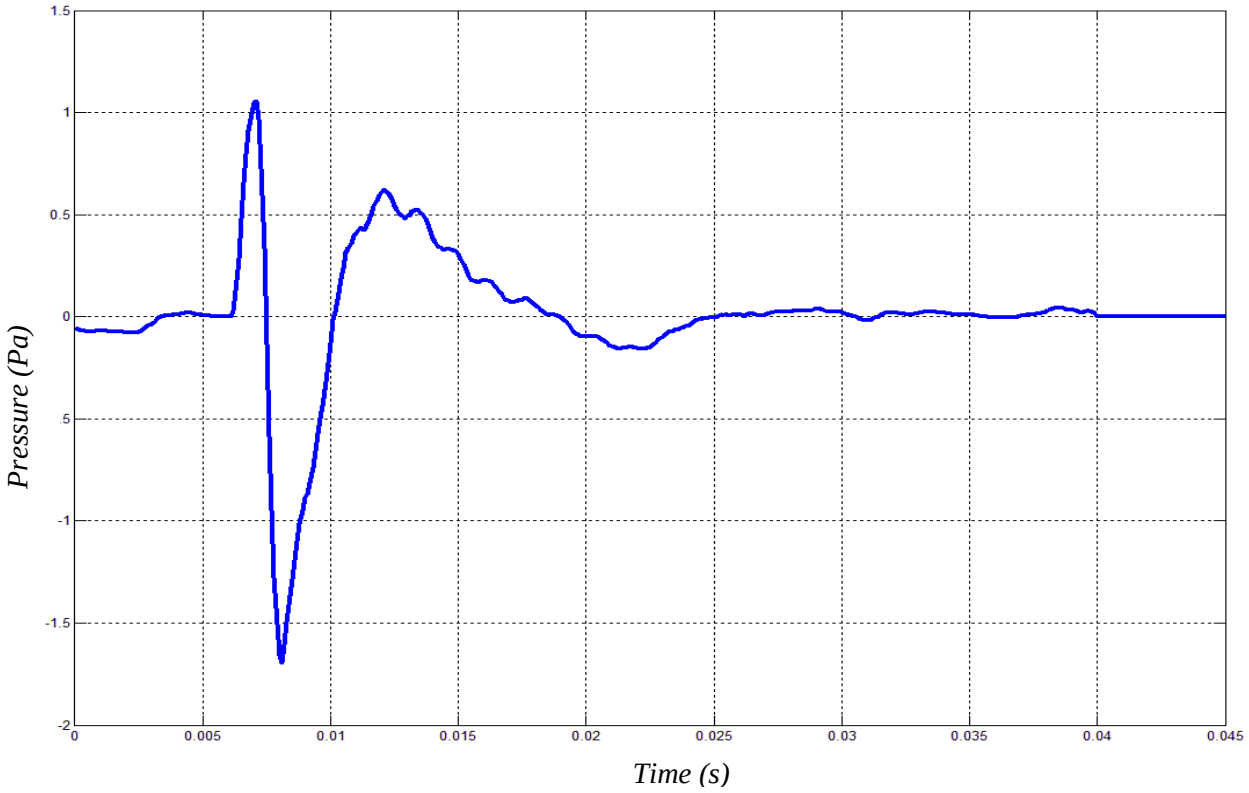

Figure 6: *Input pressure pulses generated by signal generator at 500 Hz frequency.*

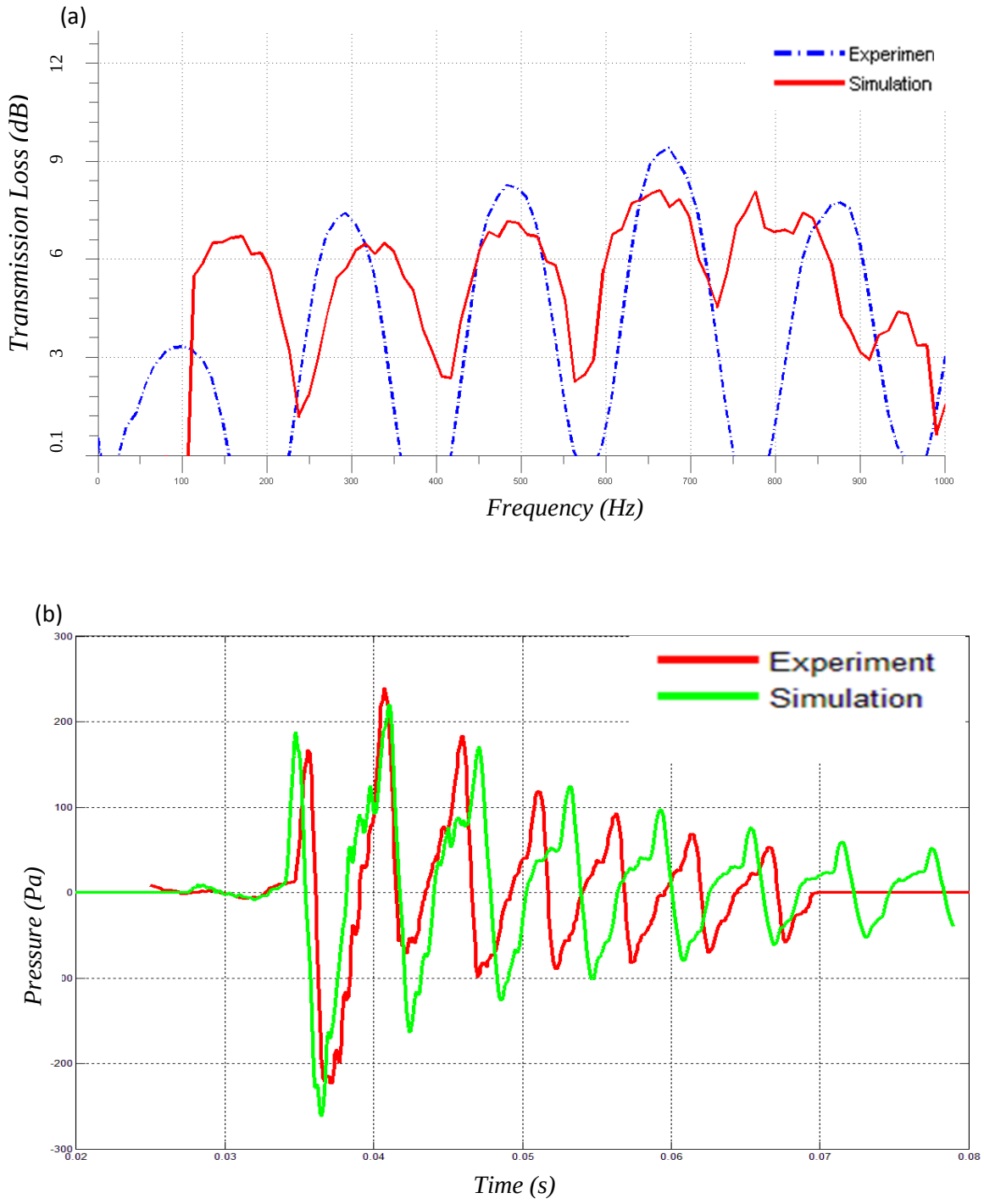

Figure 7: *(a) Comparison of Transmission loss spectrum at 500 Hz generator frequency. (b) Comparison of Transmitted pulse plot at 500 Hz generator frequency.*

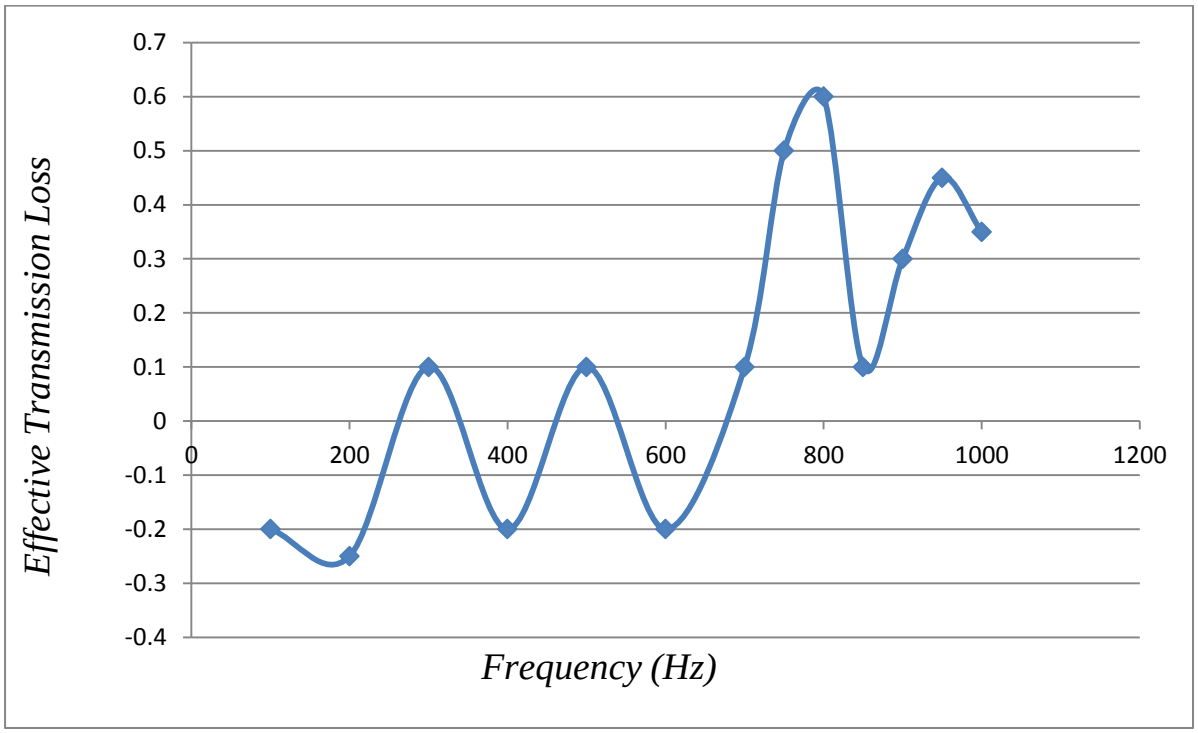

Figure 8: Effective Transmission Loss across frequency range.

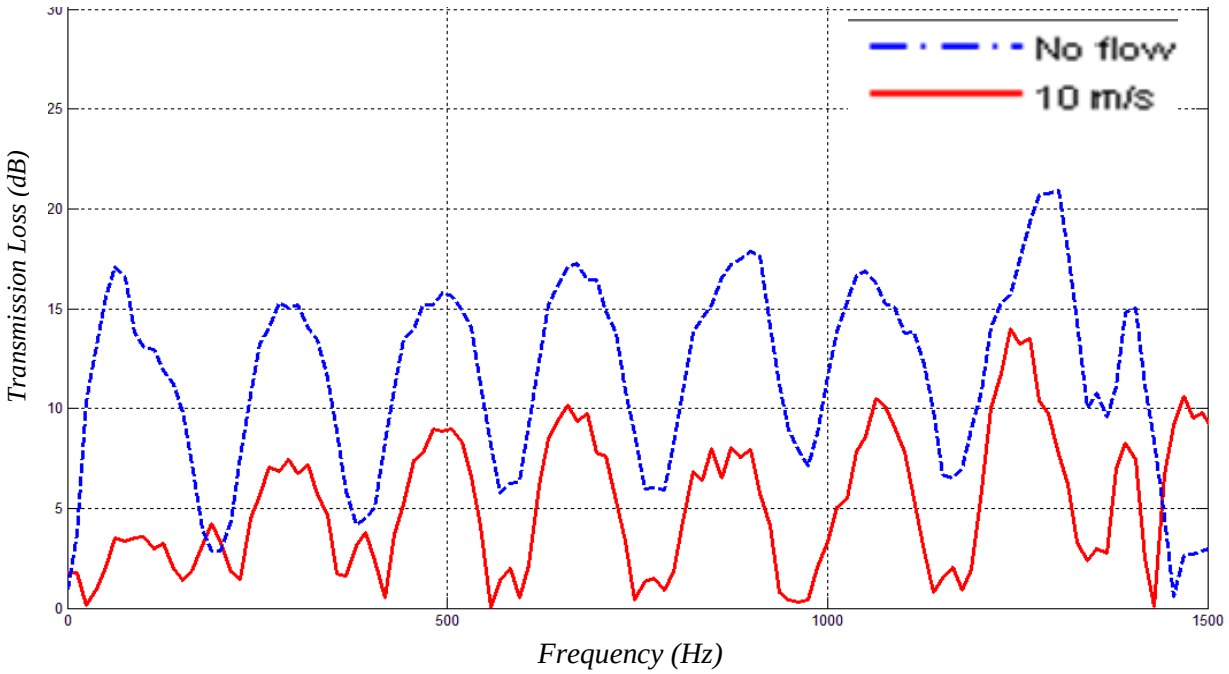

Figure 9: *Comparison of FFT of muffler without any flow and muffler at 10 m/s flow for generator frequency of 500Hz.*

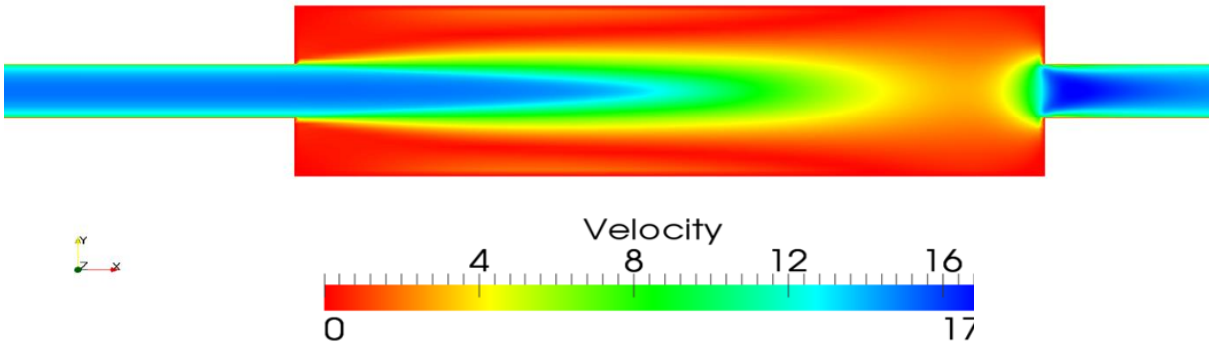

Figure 10: *Contour plot of axial velocity magnitude (m/s) for RANS simulation of muffler*

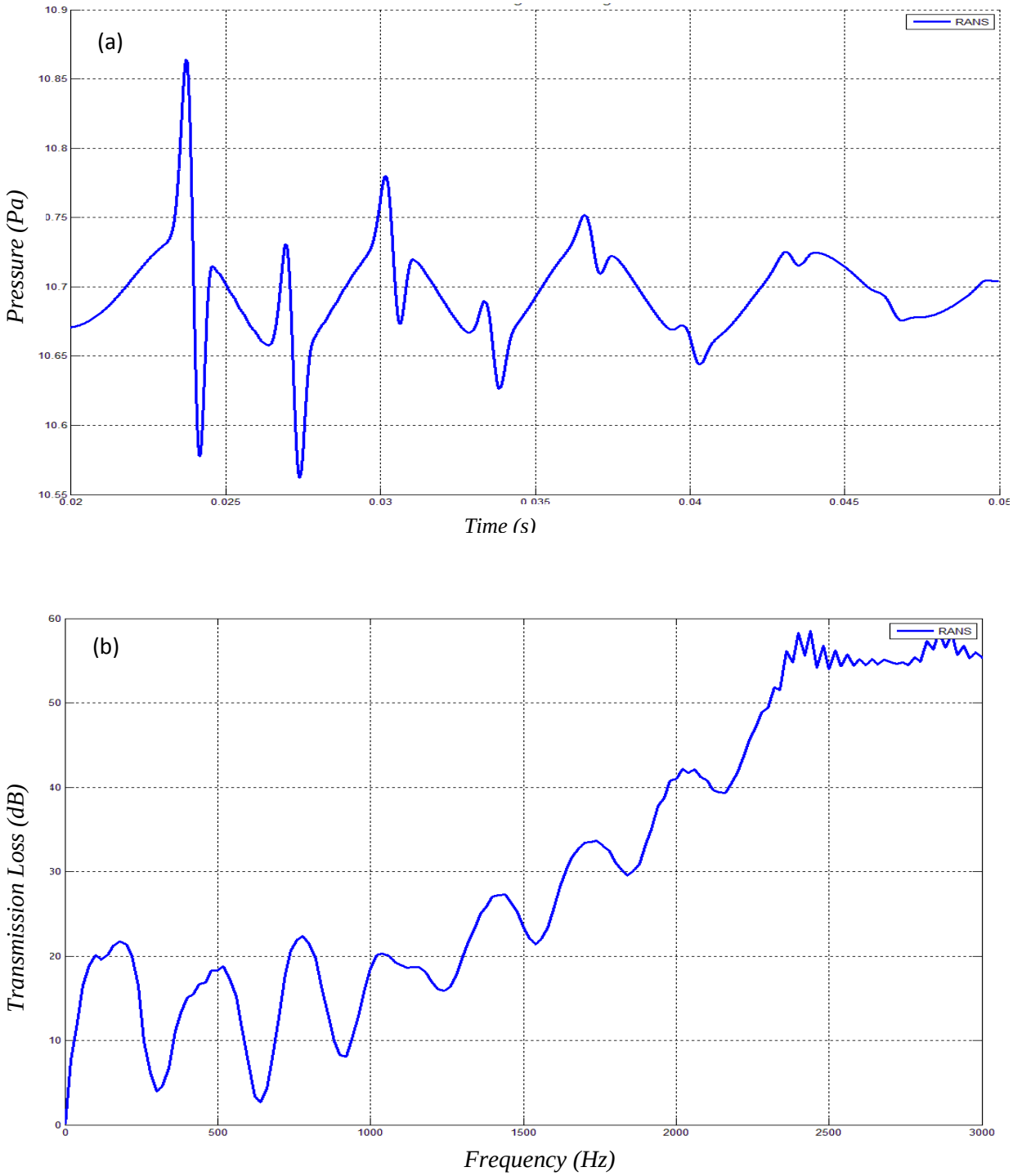

Figure 11: (a) *Transmission pressure pulse for pulse propagation in expansion muffler.* ***(b)*** *Transmission loss spectrum for pulse propagation in expansion muffler.*

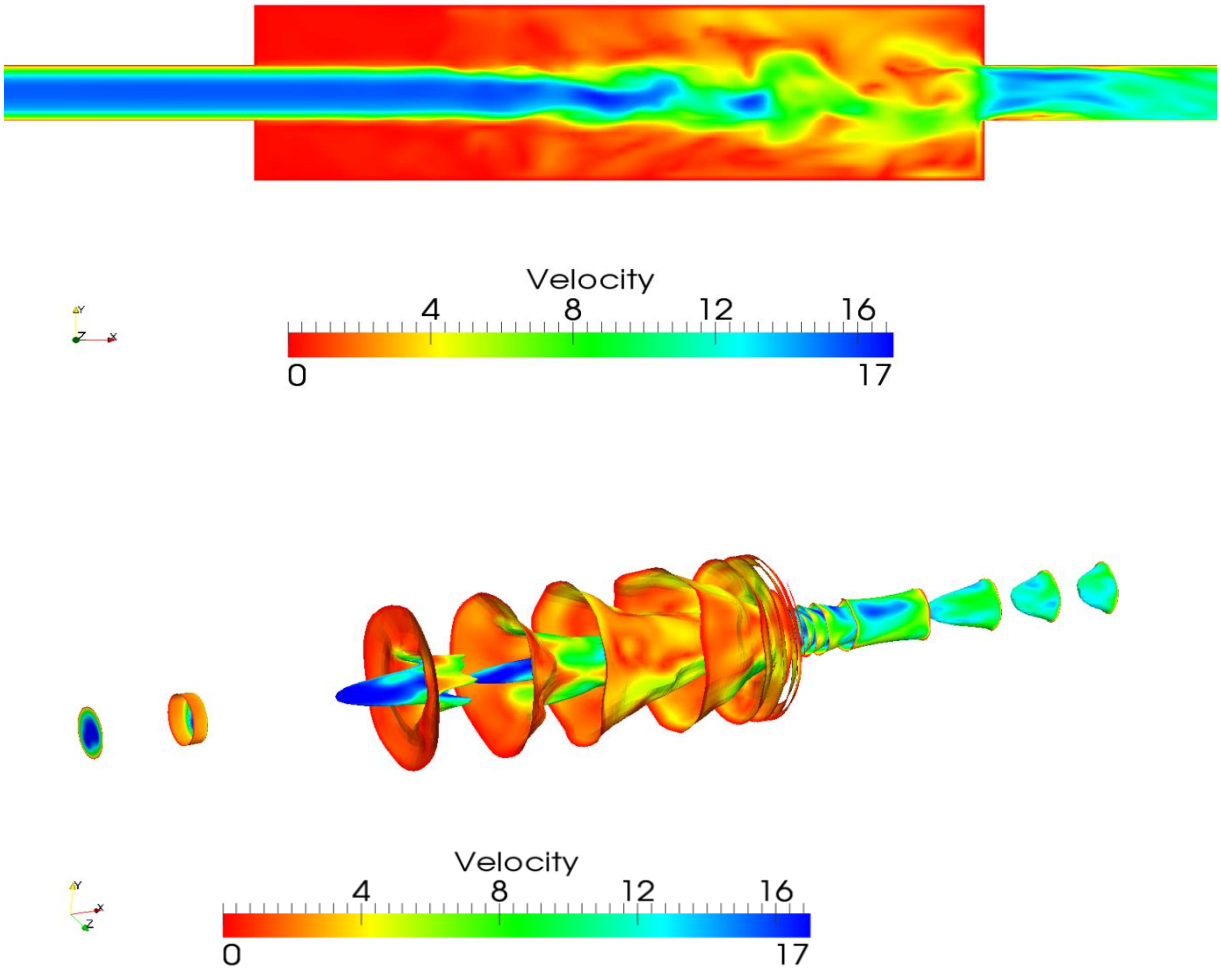

Figure 12: *Instantaneous contours of velocity magnitude (m/s) inside expansion chamber (top). Acoustic pressure (Pa) isosurface showing velocity distribution (bottom).*

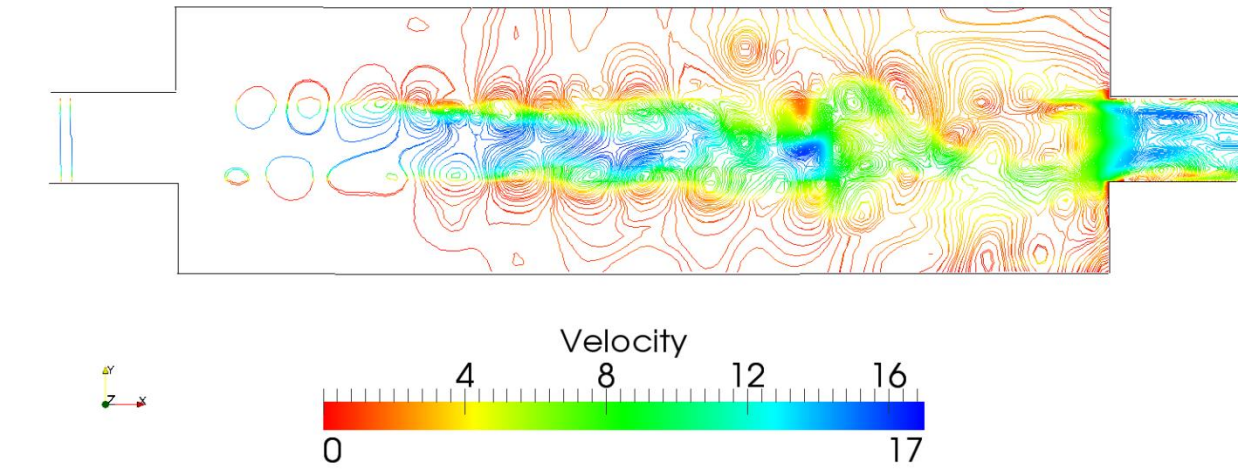

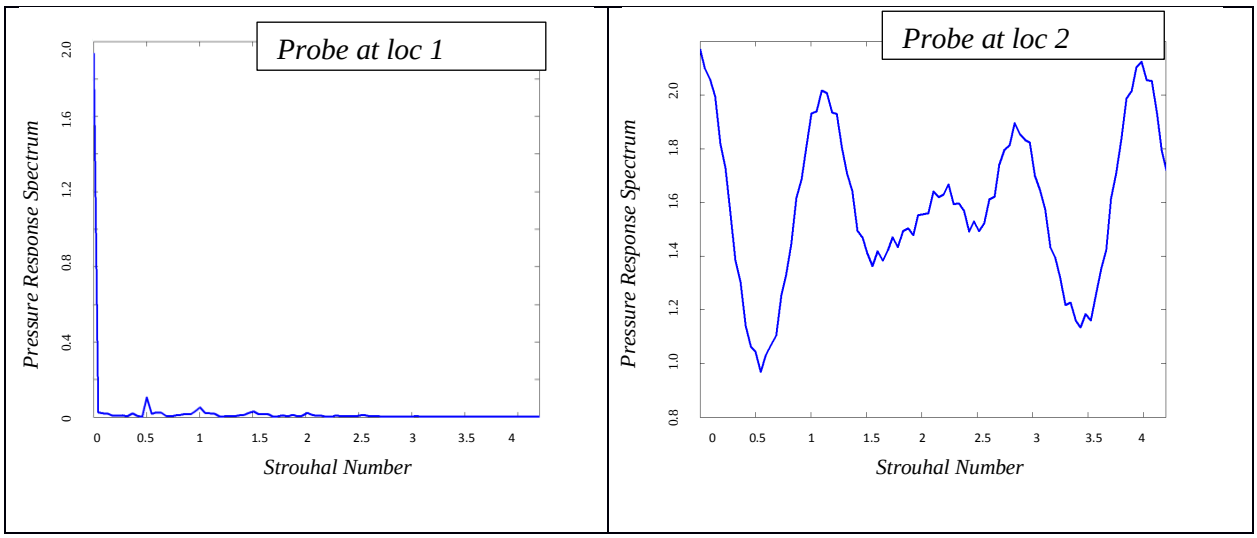

Figure 13: *Before forced pulsation: Pressure contour coloured by velocity magnitude inside expansion chamber showing vortex roll-up (top); Pressure response spectra at rear and in the middle of expansion chamber (bottom).*

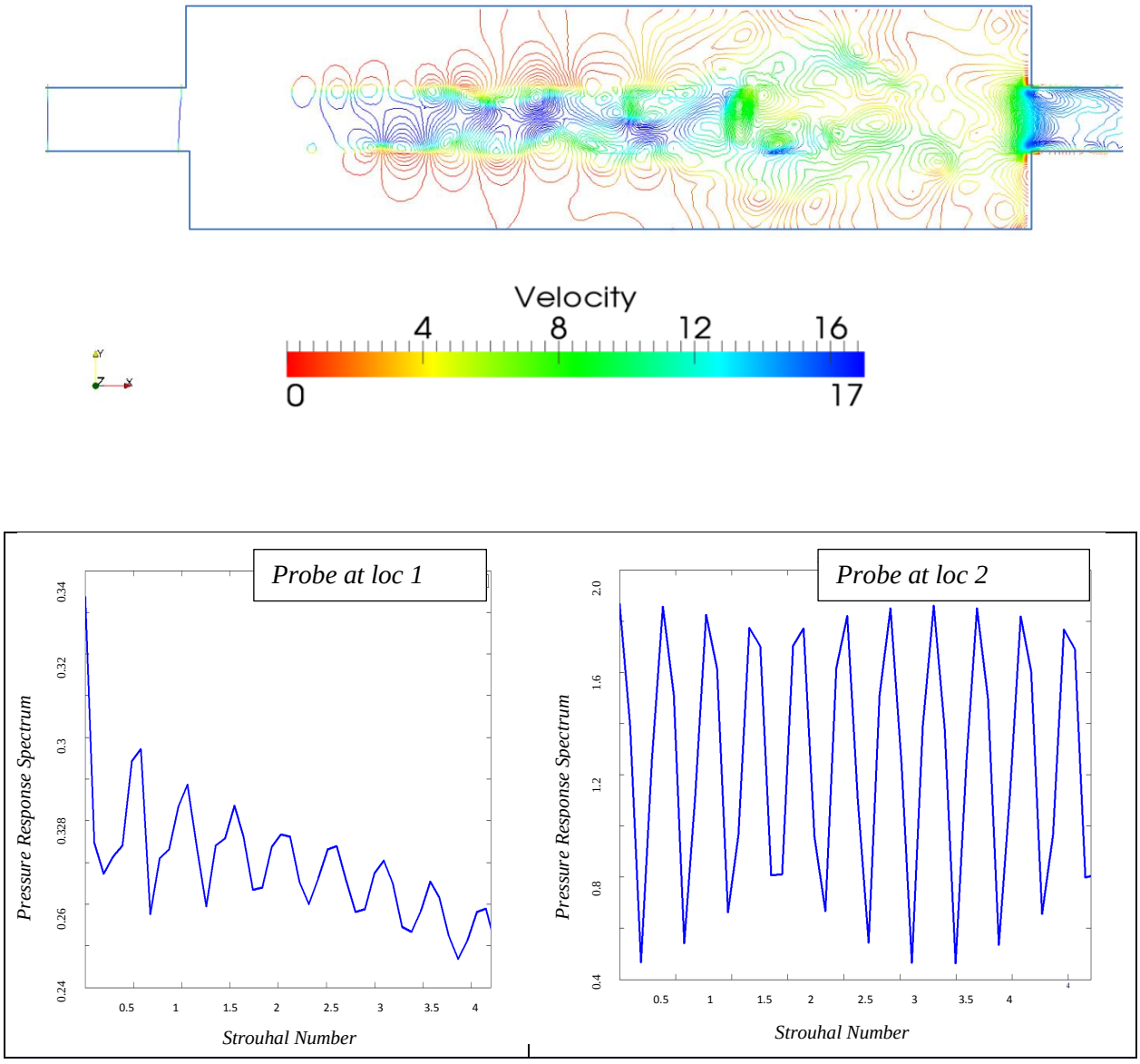

Figure 14**:** *After forced pulsation: Pressure contour coloured by velocity magnitude inside expansion chamber showing vortex roll-up (top); Pressure response spectra at rear and in the middle of expansion chamber (bottom).*

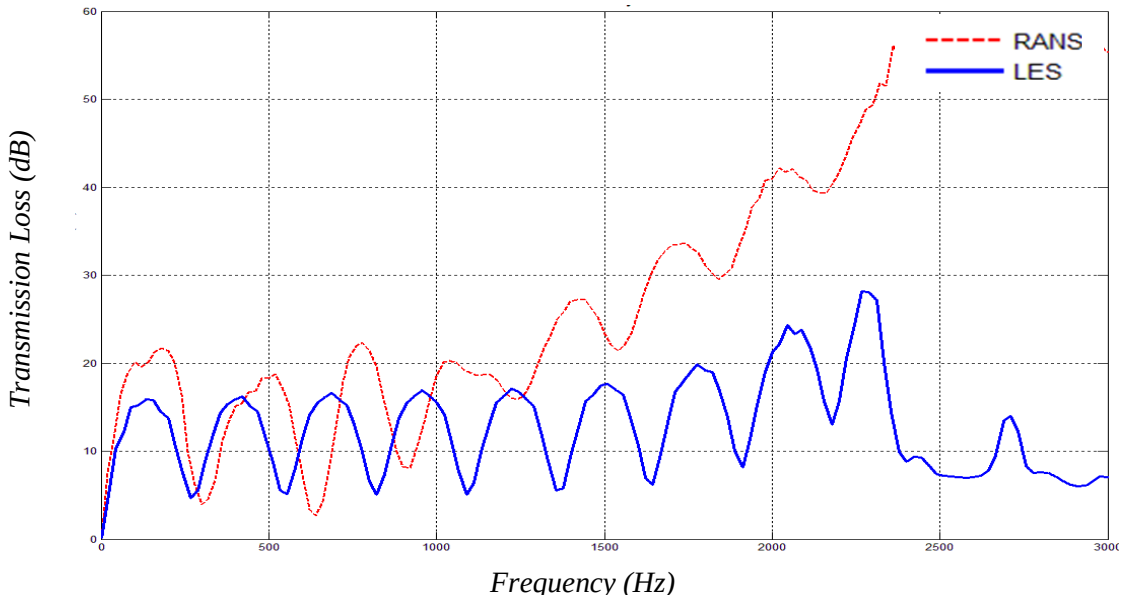

***Figure 15**: Comparison of transmission loss spectrum for RANS and LES in simple expansion muffler.*

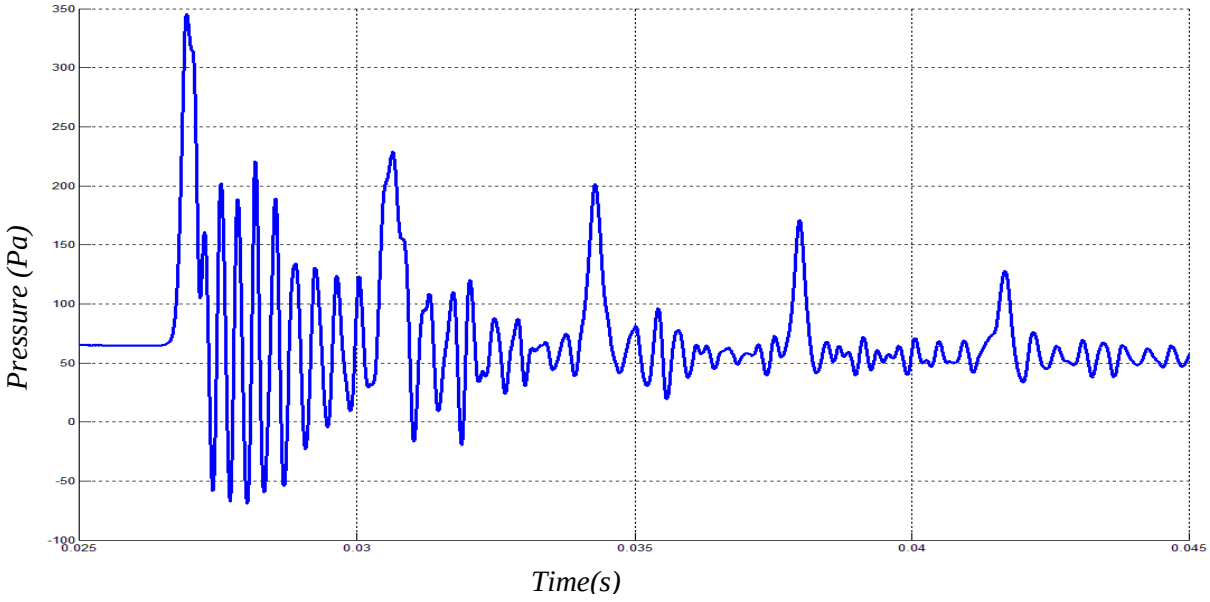

***Figure 16**: Transmission pressure spectrum of tailpipe pressure in a LES simulation of simple expansion muffler.*

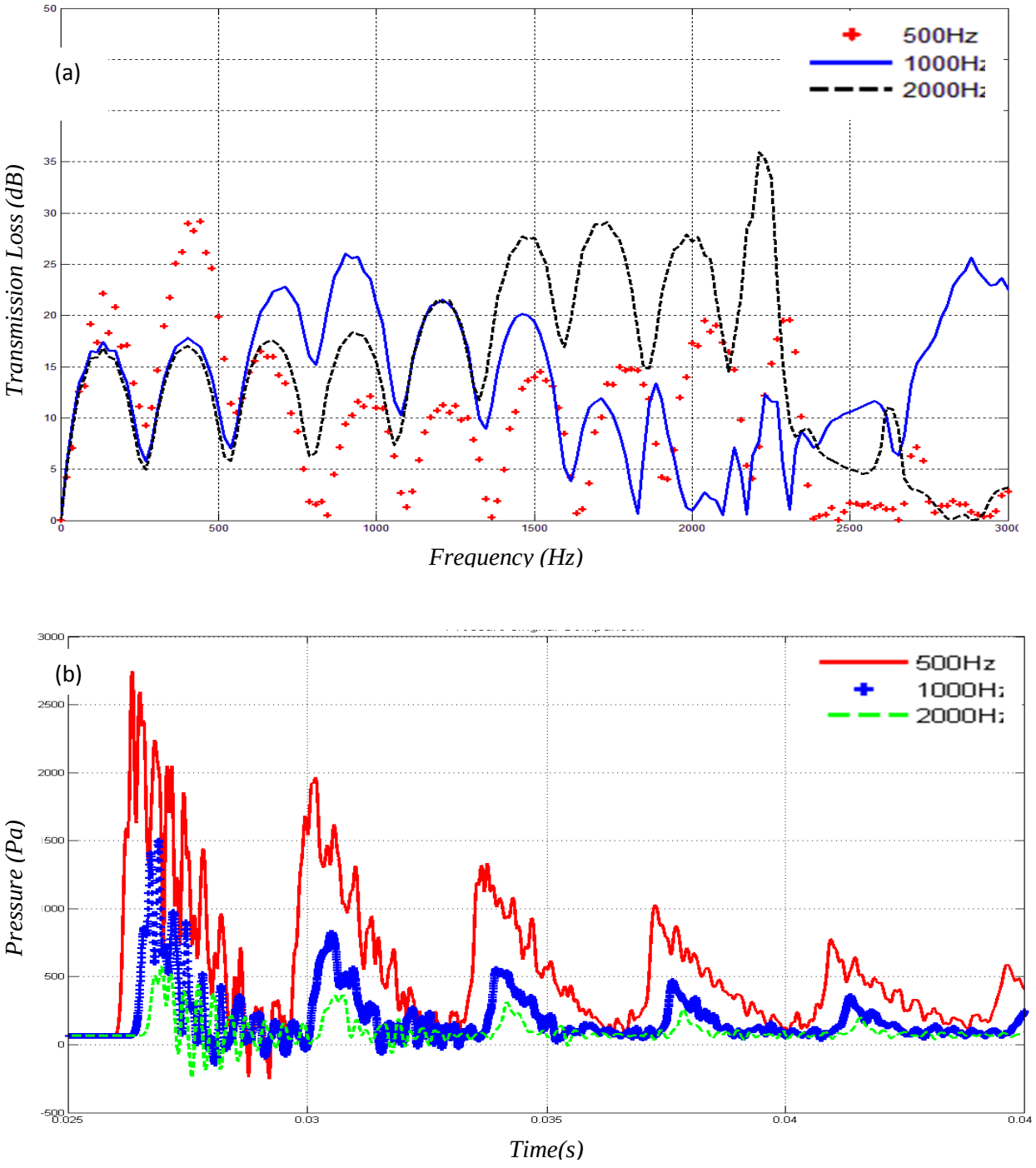

Figure 17: **(a)** *Comparison of transmission loss spectrum for various lower forced pulsation frequencies.* ***(b)*** *Comparison of transmission pulse for various lower forced pulsation frequencies. (Forced frequencies involved are 500 Hz, 1000 Hz and 2000 Hz)*